ACS OMEGA

Article

Cite This: ACS Omega 2019, 4, 5852−5861

http://pubs.acs.org/journal/acsodf

Nanometric $NaYF_4$ as an Unconventional Support for Gold Catalysts for Oxidation Reactions

Shashank Mishra,* Franck Morfin, Violaine Mendez, Prakash N. Swamy, Jean-Luc Rousset, and Stéphane Daniele

Univ Lyon, Université Claude Bernard Lyon 1, CNRS, IRCELYON—UMR 5256, 2 Avenue Albert Einstein, 69626 Villeurbanne, France

Supporting Information

ABSTRACT: The metal−support interaction plays an important role in gold catalysis. We employ here crystalline cubic (α-) and hexagonal (β-) phases of heterometallic fluoride $NaYF_4$ nanoparticles (NPs), obtained by the decomposition of a single source precursor [$NaY(TFA)_4$(diglyme)] (TFA = trifluoroacetate), as nonoxide supports for gold catalysts. Using an isostructural gadolinium analogue, we also obtained doped α-$NaYF_4$:Gd^{3+} and β-$NaYF_4$:Gd^{3+} NPs. A successful deposition of ∼1% by weight gold NPs of average size 5−6.5 nm on these doped and undoped metal fluorides using $HAuCl_4 \cdot 3H_2O$ afforded $Au/NaYF_4$ catalysts which were thoroughly characterized by using several physicochemical techniques such as X-ray diffraction, Brunauer−Emmett−Teller analysis, high-resolution transmission electron microscopy, energy-dispersive X-ray spectrometry, and X-ray photoelectron spectroscopy. A comparative study of the above catalysts for different oxidation reactions show that while for the aerobic oxidation of *trans*-stilbene in solution phase, they are either better (in terms of stilbene conversion) or at par (in terms of *trans*-stilbene oxide yield) in comparison to the reference catalyst Au/TiO_2 of the World Gold Council, their activity toward CO oxidation reactions in gas phase remains much less than that of gold catalysts supported on metal oxides.

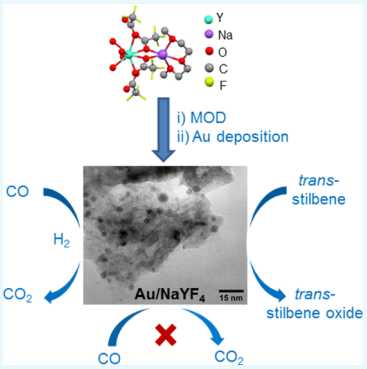

1. INTRODUCTION

Supported gold nanoparticles (NPs) continue to attract huge attention because of their relatively unexplored catalytic activity as compared to other noble metals.[1] Apart from the synthetic methods employed, the size of the gold nanoparticle, and its valence state, the nature of support is also believed to be a critical aspect in the catalytic efficiency of gold catalysts.[2] The combined effect of these factors leads to a quite complicated catalytic mechanism for the supported gold systems. Metal oxides are the most commonly used supports for the gold NPs, though some other supports such as metal−organic frameworks, carbon, and zeolites have also been employed.[3] In oxidation reactions particularly, the activation of molecular oxygen is of utmost importance, and the support should be involved in dissociating molecular oxygen at the perimeter sites of the gold particles. In metal oxide-supported gold catalysts, the metal−oxide interface plays an important role in catalytic oxidation reactions because of the geometric changes and charge transfer between the oxide support and the metal.[4] Because of the similarity in ionic radii, metal fluoride and metal oxide networks often exhibit common structural features. Nonetheless, their physical properties are different, as fluoride because of its high electronegativity forms much stronger ionic bonding in metal fluorides. Although nanometric metal fluorides have been recently used as an acidic support to anchor noble metal centers (including gold) for hydrogenation,[5] their potential as a support for oxidation reactions remains unexplored, mostly because of their perceived instability in a drastic oxidative environment and generally a low specific surface area.

In this contribution, we present the application of two different phases of $NaYF_4$, namely cubic (α-phase) and hexagonal (β-phase), as catalyst supports for Au NPs and study their catalytic performance in oxidation reactions. Among the two phases of $NaYF_4$, the α-phase is kinetically preferred but thermodynamically less stable.[6] The two phases have very different structures. The cubic $NaYF_4$ has a typical fluorite structure (CaF_2), where the Ca^{2+} sites are occupied by Na^+ and Y^{3+} ions randomly, each cation site being 8-coordinated (Figure 1a). On the other hand, the β-phase of $NaYF_4$, also written as $Na_{1.5}Y_{1.5}F_6$, has three types of cation sites: a ninefold coordinated site occupied by Y^{3+}, another ninefold coordinated site occupied randomly by 1/2 Na^+ and 1/2 Y^{3+}, and a sixfold coordinated position occupied by 1/2 Na^+ and vacancies (Figure 1b).[7]

Selection of a suitable synthetic route to these nanomaterials is crucial as the properties of the support as well as the active catalytic phase may evolve during the preparation of the catalysts.[8] The bottom-up synthesis of nanomaterials using well-defined molecular precursors offers numerous advantages

Received: January 18, 2019
Accepted: March 12, 2019
Published: March 26, 2019

DOI: 10.1021/acsomega.9b00173
ACS Omega 2019, 4, 5852−5861

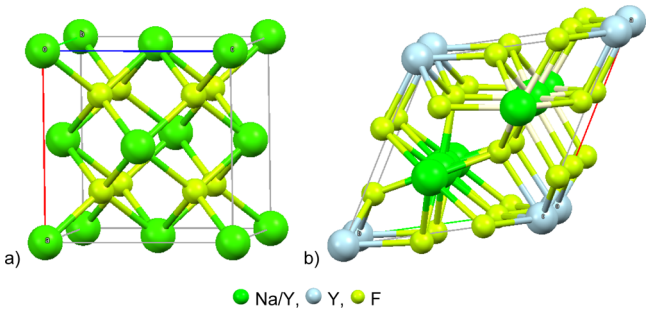

Figure 1. Crystal structures of α-$NaYF_4$ (a) and β-$NaYF_4$ (b).

over other synthetic routes.[9] However, thoroughly characterized single source precursors (SSPs) for metal fluoride nanomaterials are rather few in number.[10] Previously, we have developed anhydrous homo- and heterometallic trifluoroacetate (TFA) complexes with glyme ligands as the facile precursors to binary and ternary metal fluoride nanomaterials, mainly for upconversion and scintillation applications.[11,12] The ancillary glyme ligand not only ensures the formation of anhydrous complexes by saturating the coordination sphere of the metal centers, but also acts as a surfactant during decomposition to check the size of the metal fluoride nanocrystals and render them monodispersed in organic media. The two phases of $NaYF_4$ obtained by the above-mentioned bottom-up approach were used as supports, and polyvinyl alcohol (PVA)-protected gold NPs were deposited on them using $HAuCl_4{\cdot}3H_2O$ as the precursor. Following a previous report from this laboratory which showed an enhanced mass transfer in the Gd^{3+}-doped $Au-TiO_2$ catalysts,[13] we also doped these α- and β-phases of $NaYF_4$ with ~3 wt % Gd^{3+} ions. The purpose of doping was to improve the wettability of our catalysts in the reaction medium and, therefore, to enhance the accessibility of the gold nanoparticle to the reactants, particularly for the solution-phase reaction. Moreover, the support $NaYF_4$ is an ideal material to be doped with Gd^{3+} because of the compatibility of the Y^{3+} and Gd^{3+} ions.[14] The obtained Au/α-$NaYF_4$, Au/β-$NaYF_4$, Au/α-$NaYF_4$:Gd^{3+}, and Au/β-$NaYF_4$:Gd^{3+} catalysts were thoroughly characterized by using several physicochemical techniques such as X-ray diffraction (XRD), Brunauer–Emmett–Teller (BET) analysis, high-resolution transmission electron microscopy (HRTEM), energy-dispersive X-ray (EDX) spectrometry, and X-ray photoelectron spectroscopy (XPS). The catalytic efficiency of these materials was subsequently evaluated in the aerobic epoxidation of *trans*-stilbene in methylcyclohexane as well as carbon monoxide (CO) and H_2 oxidation in the gas phase.

2. RESULTS AND DISCUSSION

2.1. Synthesis and Characterization of $NaYF_4$ Supports and Au/$NaYF_4$ Catalysts. The molecular precursor [$NaY(TFA)_4$(diglyme)] [where TFA = trifluoroacetate; diglyme = bis(2-methoxyethyl) ether] starts decomposing in 1-octadecene at 250 °C to give only α-$NaYF_4$ nanocrystals (JCPDS: 077-2042) (Scheme 1).[12] Because of the presence of the diglyme ligand, provided in situ by the precursor molecule, no additional surfactant was needed for the size control of these $NaYF_4$ NPs. At a higher temperature, α- and β-mixed phases are obtained, the relative ratio of the two phases being dependent on the reaction temperature. A pure β-phase (JCPDS: 16-0334) is obtained by calcination of the mixed-phased NCs at 400 °C in a thermodynamically controlled process.[6] Owing to the presence of the diglyme ligand on the surface, as confirmed by the infrared (IR) spectrum and thermogravimetric and differential thermal analyses (TG–DTA) (Figures S1 and S2 in the Supporting Information), the α-$NaYF_4$ nanocrystals could be dispersed in organic solvents. However, the diglyme surfactant is mostly eliminated from the surface of β-$NaYF_4$ upon calcination at 400 °C, which is

Scheme 1. Synthesis and Characterization of the α- and β-Phases of the Support $NaYF_4$: molecular Structure of the SSP (a), XRD (b), and TEM Image (c) of α-$NaYF_4$ Obtained at 250 °C; XRD Pattern (d) and TEM Image (e) of β-$NaYF_4$ Obtained at 400 °C. Insets Show the HRTEM Images Depicting the Reticular Planes and Thus Confirming the Crystalline Nature of These Supports

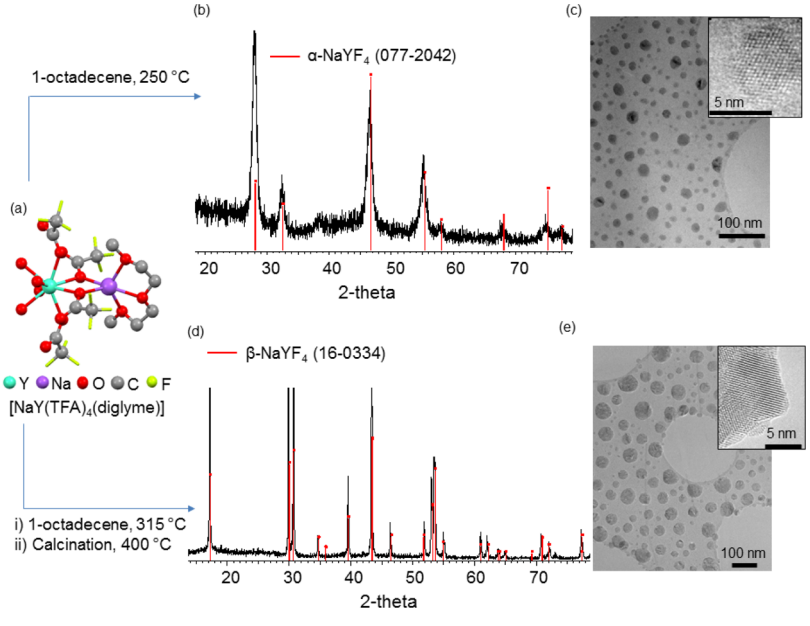

DOI: 10.1021/acsomega.9b00173
ACS Omega 2019, 4, 5852–5861

accompanied by a decrease in the dispersibility of the NCs in organic solvents and a slight increase in the average particle size. The TEM images show well-crystallized particles of sub-30 nanometric size. The HRTEM images, presented in the insets of Scheme 1, clearly show lattice fringes, thus confirming the high crystallinity of these particles. This analysis also confirms the phase-pure single crystal nature of α- and β-$NaYF_4$ NPs.

Previous studies have shown that doping a metal oxide support with Gd^{3+} improves the catalytic efficiency of the gold catalysts in terms of enhanced wettability and mass transfer.[13] Therefore, we also synthesized two Gd^{3+}-doped supports, that is, α-$NaYF_4$:3.7 mol % Gd^{3+} and β-$NaYF_4$:4.2 mol % Gd^{3+} (where the values of mol % refer to the atomic substitution ratio of Y^{3+} by Gd^{3+}) by decomposing simultaneously the solutions of two isostructural Na−Y and Na−Gd precursors [$NaLn(TFA)_4$(diglyme)] (Ln = Y, Gd) taken in appropriate ratios. Compared to the Na−Y precursor, the Na−Gd analogue gives the β-phase of $NaGdF_4$ NCs on decomposition in 1-octadecene at 280 °C.[12] The different decomposition behavior of isostructural [$NaLn(TFA)_4$(diglyme)] (Ln = Y and Gd) is attributed to the fact that the slightly larger Gd^{3+} (r = 1.11 Å for 9-coordination) ions can be accommodated in the β-phase easily as compared to the Y^{3+} ions (r = 1.07 Å for 9-coordination).[14a] Previously, Liu et al. observed the α-to-β phase transition simply by doping $NaYF_4$ with larger Gd^{3+} cations (30 mol %).[14b] However, a small doping of around 4 mol % here does not change the crystalline phases of $NaYF_4$, as confirmed by powder XRD studies (Figures S3 and S4).

The above two phases of $NaYF_4$ behaved differently during the colloidal deposition of PVA-protected gold NPs using $HAuCl_4{\cdot}3H_2O$ as the precursor. Although gold loading of 0.77 and 0.94 wt % could be achieved within 1 h for α-$NaYF_4$ and α-$NaYF_4$:Gd^{3+}, respectively, it took about 12 and 16 h of reaction time for the loading of 0.72 and 0.85 wt % in the case of β-$NaYF_4$ and β-$NaYF_4$:Gd^{3+}, respectively. The XRD patterns of the α-$NaYF_4$ and β-$NaYF_4$ phases before and after the deposition of gold NPs were similar, indicating that the presence of gold does not alter the structures of the two supports (Figures S3 and S4). No peaks for gold NPs were observed in the XRD patterns, which is consistent with the previous observation that, unless the Rietveld method is employed for the refinement of crystalline structure, highly dispersed gold NPs cannot be detected by XRD.[8] The particle size distribution histograms, as obtained by direct observation of the TEM images, show a relatively narrow size distribution for the gold NPs (Figures 2 and 3). From these TEM images, average gold particle sizes of 6.5 and 4.9 nm were calculated for α-$NaYF_4$ and β-$NaYF_4$, respectively. On the other hand, there was no marked difference in the average size of gold NPs for the two doped catalysts (5.1 nm for both α-$NaYF_4$:Gd^{3+} and β-$NaYF_4$:Gd^{3+}). The HRTEM images clearly show the lattice fringes of highly crystalline gold NPs. The EDX analyses confirmed the presence of all the elements expected in these catalysts, that is, Na, Y, Gd (in case of doped catalysts), F, Au, O, and C (Figure S5). The nitrogen adsorption−desorption isotherm measurements were performed on all the catalysts prepared here to evaluate their surface characteristics. The BET surface area and BJH average pore diameter for the Au/α-$NaYF_4$ catalyst were found to be 96 m^2/g and 6.1 nm, respectively (Figure S6). Generally speaking, $NaYF_4$ and related materials exhibit a low surface area (typically less than 15 m^2/g).[15] No doubt, the high surface area observed here is due to the surface-passivating effects of the diglyme ligand, which results in the formation of small NPs and an imperfect packing for them. On doping with Gd^{3+}, however, the surface area decreases to 11 m^2/g. In contrast, the catalysts based on both doped and undoped β-$NaYF_4$ supports show a poor BET specific surface area (4−9 m^2/g). Some important data on the above-obtained Au/$NaYF_4$ materials are collected in Table 1.

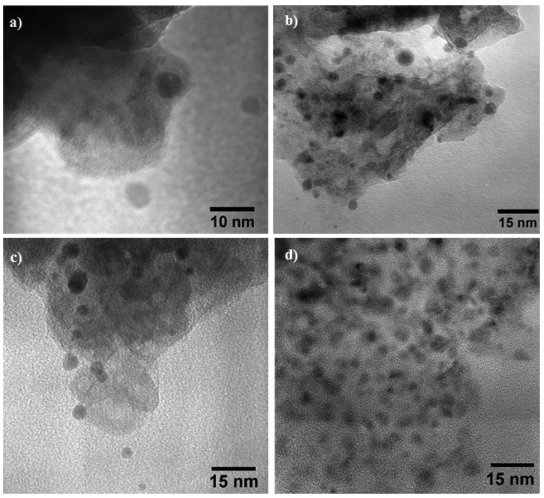

Figure 2. Representative TEM images of the four differently supported Au catalysts: (a) Au/α-$NaYF_4$, (b) Au/β-$NaYF_4$, (c) Au/α-$NaYF_4$:Gd^{3+}, and (d) Au/β-$NaYF_4$:Gd^{3+}.

To have a better understanding of the interaction between the gold NPs and fluorinated supports, the XPS studies were conducted on all the four catalysts as well as the support $NaYF_4$ itself. The wide scan spectra reveal the co-presence of gold, sodium, yttrium, fluorine, oxygen, carbon, and, in case of doped catalysts, gadolinium elements (Figures S7−S11, Tables 2 and S1). The binding energy values were corrected for surface charging by taking the C 1s peak of contaminant carbon as a reference at 284.6 eV, as the C 1s peak of adventitious carbon species or carbon from the PVA ligand are both located very close to this value.[16] The core-level spectra in the Au 4f region show binding energies at 82.4−83.4 eV (Au $4f_{7/2}$), which can be assigned to metallic Au, as no peaks because of the oxidized species, usually found at about 85.5 and 86.3 eV,[17] were detected (Figure 4). These values show significant shifts toward lower binding energies, as compared to the value for the bulk metallic gold (84.0 eV), which is in accordance with the previous results by Duo et al.[18] Interestingly, we observed a splitting of the characteristic Au 4f bands for gold deposited on β-$NaYF_4$ supports (Figure 4b,d), where the $4f_{7/2}$ and $4f_{5/2}$ are both decomposed into two components. The prominent bands, marked as 1 and 2 in Figure 4, should correspond to the core Au atoms, whereas the bands with low intensities, designated as 3 and 4, are due to the modified surface Au atoms bonded to the "O−C" group at the Au−PVA interface.[19] This indicates that, in particular cases where deposition of the PVA-protected gold NPs took a longer time period, washing the sample with water was not sufficient to remove the PVA ligand entirely.

2.2. Catalytic Activity of Au/$NaYF_4$ Catalysts. To determine the potential of these nanometric metal fluorides as nonoxide supports for gold catalysts, the catalysts Au/α-$NaYF_4$, Au/β-$NaYF_4$, Au/α-$NaYF_4$:Gd^{3+}, and Au/β-

DOI: 10.1021/acsomega.9b00173
ACS Omega 2019, 4, 5852−5861

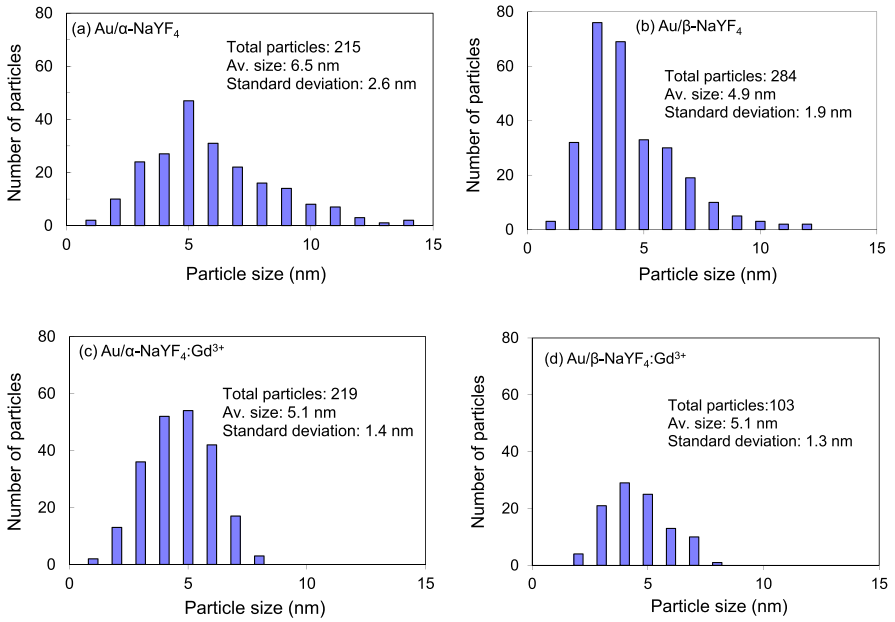

Figure 3. Gold particle size distribution in the catalysts (a) Au/α-$NaYF_4$, (b) Au/β-$NaYF_4$, (c) Au/α-$NaYF_4$:Gd^{3+}, and (d) Au/β-$NaYF_4$:Gd^{3+}.

Table 1. Some Properties of the Au/$NaYF_4$ Catalysts Prepared Using SSPs

	catalyst	temp. support obtained (°C)	crystallite size of support (by Scherrer's eqn in XRD, nm)	BET surface area (m^2/g)	Au loading (wt %), deposition time (h)	% Gd(wt)	av. Au NP size (TEM, nm)	av. Au NP size ($D_{3/2}$ Sauter, nm)	Au dispersion
1	Au/α-$NaYF_4$	250	10	96	0.77, 1		6.5	8.6	0.14
2	Au/β-$NaYF_4$	400	30	4	0.72, 12		4.9	6.7	0.18
3	Au/α-$NaYF_4$:Gd^{3+}	250	10	11	0.94, 1	3.1	5.1	5.8	0.20
4	Au/β-$NaYF_4$:Gd^{3+}	400	55	9	0.85, 16	3.5	5.1	5.8	0.20

Table 2. Selected Au 4f XPS Data of Au/$NaYF_4$ Catalysts

		Au $4f_{7/2}$			Au $4f_{5/2}$		
		fitted peak	component peaks		fitted peak	component peaks	
	sample		1	3		2	4
2.	Au/α-$NaYF_4$	83.3			87.0		
3.	Au/β-$NaYF_4$	83.3	83.1	84.2	86.9	86.7	87.7
4.	Au/α-$NaYF_4$:Gd^{3+}	83.2			86.8		
5.	Au/β-$NaYF_4$:Gd^{3+}	82.5	82.4	82.9	86.2	86.0	86.6

$NaYF_4$:Gd^{3+} were tested for the aerobic epoxidation of stilbene in methylcyclohexane and CO and H_2 oxidation in gas phase under the standard conditions developed for these reactions.[20,21] These two catalytic reactions are merely used as probes to highlight the potentials of the synthesized metal fluorides as supports for gold NPs, and the various catalytic behaviors observed are simply discussed in the light of previous works.

2.2.1. Aerobic Epoxidation of trans-Stilbene. As expected for supported gold NPs with diameters of about 5 nm, all of the catalysts described above show catalytic activity in the aerobic epoxidation of *trans*-stilbene in methylcyclohexane.[22] The description of the current understanding of the reaction mechanism can be found elsewhere.[23] With 92% conversion and 49% epoxide yield after 100 h, Au/α-$NaYF_4$ is the least active catalyst of the series, which is consistent with the larger size of the gold NPs (6.5 nm) in this catalyst. For all other catalysts, namely Au/β-$NaYF_4$, Au/α-$NaYF_4$:Gd^{3+}, and Au/β-$NaYF_4$:Gd^{3+}, which have an average gold particle size of ∼5 nm, full stilbene conversion was achieved in 100 h, together with a *trans*-stilbene oxide yield of 54−63% (Figures 5 and 6). For these catalysts, 40−47% of epoxide is readily formed within 48 h, at 74−87% stilbene conversion. These values are either at par (in terms of *trans*-stilbene oxide yield) or better (in terms of stilbene conversion) than that for the World Gold Council (WGC) reference catalyst Au/TiO_2 for which 46% epoxide is formed after 48 h at a conversion of 65%. These values are many times more than the maximum 5% epoxide yield expected from the sole action of *tert*-butyl hydroperoxide (TBHP) as an oxidant/oxygen donor for the alkene, thus indicating the involvement of molecular oxygen from the air in the epoxidation process. The support itself does not contribute to the high activities observed for these Au/$NaYF_4$ catalysts, as α-$NaYF_4$ alone yields only a negligible amount of epoxide in 24 h. In all cases, epoxide is the main product obtained in the aerobic process, along with some other minor products such as benzaldehyde, deoxybenzoin, and benzil (less than 5% of the total product). Two types of catalytic profiles were observed:

DOI: 10.1021/acsomega.9b00173
ACS Omega 2019, 4, 5852−5861

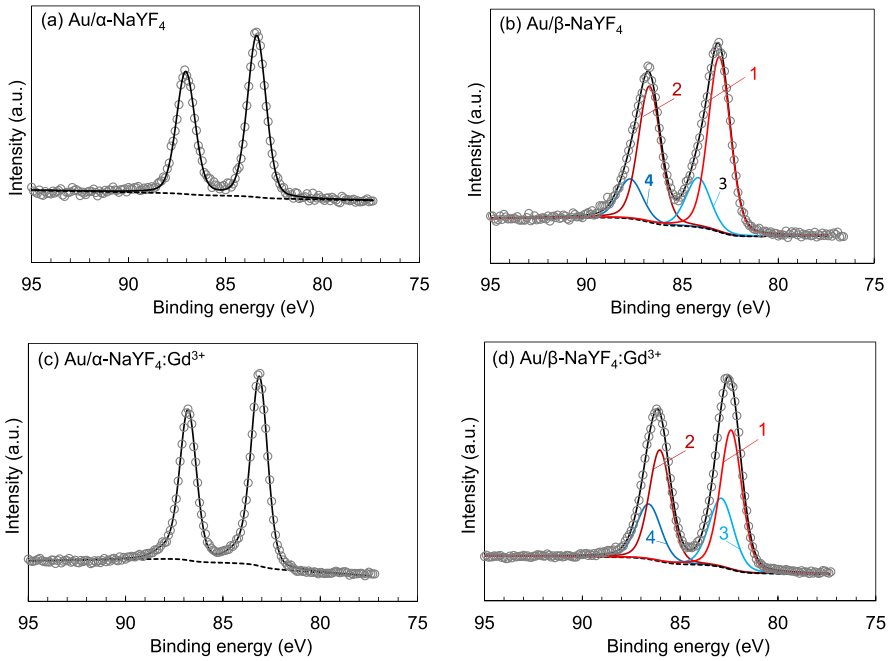

Figure 4. Au 4f XPS spectra of the four differently supported Au catalysts: (a) Au/α-$NaYF_4$, (b) Au/β-$NaYF_4$, (c) Au/α-$NaYF_4$:Gd^{3+}, and (d) Au/β-$NaYF_4$:Gd^{3+}. The binding energies of Au 4f were corrected by taking the C 1s peak as a reference at 284.6 eV.

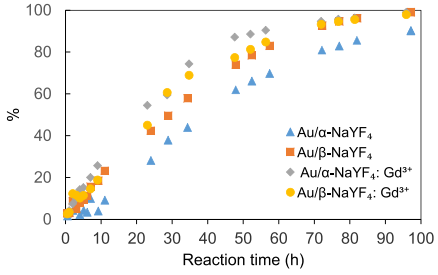

Figure 5. *trans*-Stilbene conversion observed over $Au/NaYF_4$ catalysts. Reaction conditions: *trans*-stilbene (1 mmol), methylcyclohexane (20 mL), catalyst (2.1 ± 0.1 μmol Au), TBHP (0.05 mmol), air (1 atm), 80 °C, 900 rpm.

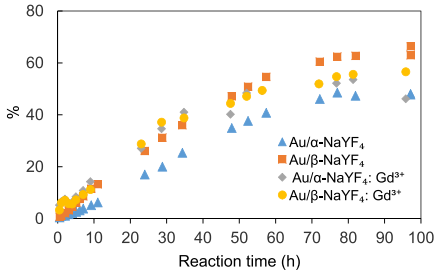

Figure 6. Epoxide yield observed over $Au/NaYF_4$ catalysts. Reaction conditions are specified in the caption of Figure 5.

catalysts supported on the undoped $NaYF_4$ show an induction period, as observed previously on the Au/TiO_2:Gd^{3+} and $Au/Al_4Ga_2O_9$ catalysts.[8,13] This can be attributed to a possible conditioning of the catalyst in the reaction, for example, to a reaction between the peroxide initiator and the catalyst surface.[24] After conditioning, the epoxidation rates reach 0.018 and 0.032 mol g_{Au}^{-1} h^{-1} in the case of Au/α-$NaYF_4$ and Au/β-$NaYF_4$ catalysts, respectively (Table 3). By taking into consideration the dispersion of gold (Table 1), which is determined from the volume/surface-weighted mean diameter d_{32} (also called the Sauter diameter) by mathematical models assuming a cubo-octahedron geometry of the particle,[25] the turnover frequencies (TOFs) are calculated to be 27−34 h^{-1}. These values are 1.7−1.8 times higher than those found during the initial induction period. The maximum epoxidation rate observed (after the induction period) for Au/β-$NaYF_4$ is about 2 times higher than that for Au/α-$NaYF_4$, but is slightly lower than that observed for the WGC reference catalyst Au/TiO_2. In fact, this induction period was not found when a second batch of *trans*-stilbene (1 mmol) was added after 90−95% conversion of the first 1 mmol batch. The conversion of the second batch started just after its addition and was fully converted at about the maximal rate achieved during the transformation of the first batch, that is, 27−34 h^{-1}. These experiments confirm the stability/durability of the catalyst under these mild oxidative conditions. Gold particles supported on two Gd^{3+}-doped $NaYF_4$, on the other hand, do not display any induction period. Similar behavior was

Table 3. Catalytic Data on Stilbene Epoxidation by the $Au/NaYF_4$ Catalysts

catalyst	conversion (48 h, %)	yield (48 h, %)	selectivity (48 h, %)	epoxy. rate (mol g_{Au}^{-1} h^{-1})	TOF (h^{-1})
Au/α-$NaYF_4$	62	35	57	0.0115 (induct.)/0.0185 (max.)	16 (induct.)/27 (max.)
Au/β-$NaYF_4$	74	47	64	0.0180 (induct.)/0.0321 (max.)	19 (induct.)/34 (max.)
Au/α-$NaYF_4$:Gd^{3+}	87	40	46	0.0400 (max.)	39 (max.)
Au/β-$NaYF_4$:Gd^{3+}	78	45	58	0.0316 (max.)	31 (max.)

DOI: 10.1021/acsomega.9b00173
ACS Omega 2019, 4, 5852−5861

previously observed for gold NPs supported on the group 13 homometallic oxides M_2O_3 (M = Ga, In) or mesoporous structures.[8,26] They are active from the beginning of the reaction, with the initial epoxidation rates between 0.032 and 0.040 mol g_{Au}^{-1} h^{-1}, which correspond to the TOF of 31 to 39 h^{-1} (Table 3).

Despite the relatively smaller surface area and somewhat larger gold particles in these metal fluoride-supported catalysts (5−6.5 nm) than those found in the typical metal oxide-supported gold catalysts (3−4 nm), the metal fluoride-supported catalysts described here are less selective. However, unlike some of the metal oxide-supported gold catalysts,[8] the selectivity of these catalysts remains stable throughout the reaction. With a selectivity of 46% after 48 h, Au/α-$NaYF_4$:Gd^{3+} was the least selective catalyst in the series, others showing a selectivity of 57−64%. Doping the support $NaYF_4$ with Gd^{3+} not only eliminates the induction period but also enhances the catalytic activity as indicated by larger TOF values. However, the selectivity seems to be affected by this doping. This decrease in selectivity in the two Gd^{3+}-doped $NaYF_4$ catalysts is in contrast with the previous report where such doping caused an enhancement in the selectivity of the Au/TiO_2 catalyst.[13] In particular, Au/α-$NaYF_4$:Gd^{3+} exhibits an unusually high density of gold NPs on the surface because of a high gold loading (0.94 wt %) and a low surface area (11 m^2/g). Hence, if selectivity is controlled by the support surface chemistry, as suggested previously,[27] and if selectivity is compromised by the reactions involving surface hydroxyl groups, then a low ratio of −OH/Au NP is expected to be favorable to selectivity by minimizing such parasitic reactions. These results suggest that the support, in addition to controlling the mass transfer, also plays a role in selectivity.

2.2.2. CO Oxidation. Since the discovery of the astonishingly high catalytic efficiency shown by the supported gold NPs for the oxidation of CO at low temperature,[28] numerous studies on gold NPs deposited on metal oxide supports have been pursued.[2,4] However, there is still a debate on (i) the influence of gold particle size and its charge state, (ii) effect of support, and (iii) the nature of the active site, particularly in what way and on which site O_2 is activated. The general consensus is that neutral gold particles alone cannot activate the O−O bond without some assistance from the support in terms of charge-transfer processes or involvement of specific sites at the interface. Until now, only a few reports on the catalytic studies of gold NPs on nonoxide supports such as carbon or carbon nitride materials have appeared, and none of them showed any appreciable catalytic activity for the oxidation reactions.[29,30] This low activity has been attributed to the lack of basic surface OH groups.[30]

To study the behavior of "nonoxide support"-based gold catalysts toward CO oxidation reactions in gas phase, we tested these $Au/NaYF_4$ catalysts for three catalytic reactions, that is, (i) oxidation of CO, (ii) selective oxidation of CO promoted by H_2, and (iii) oxidation of H_2. Except for the change in the incoming gas mixture, the same protocol was used for these reactions. The catalytic tests were carried out in a flow reactor at temperatures from 25 to 250 °C under atmospheric pressure using 50 N mL min^{-1} total flow of reactants in helium carrier gas. Several reaction cycles, each consisting of alternative heating and cooling periods, were recorded to monitor possible hysteresis, deactivation, or activation. For all samples, the results of the first run were significantly different from those of the subsequent cycles. This is illustrated in Figure 7 for CO

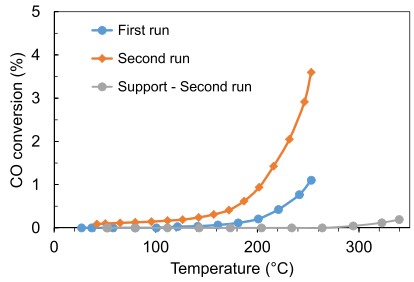

Figure 7. CO conversion as a function of temperature over the β-$NaYF_4$ support and the Au/β-$NaYF_4$:Gd^{3+} catalyst during the first and second cooling runs in CO oxidation (H_2-free mixture).

oxidation on the Au/β-$NaYF_4$:Gd^{3+} catalyst. These catalysts apparently need a thermal activation, probably because of the inhibitory effect of the capping ligand (PVA) that is still present around the catalyst, as shown by XPS results. However, the data obtained on the second and third run were similar, indicating that organic species were eliminated during the first heating cycle and that the catalyst was now stable under the reaction conditions used. Indeed, it has been shown previously that calcination at 250 °C removes the PVA ligand from the PVA-protected gold NPs.[31] It should be noted that the two phases of the support itself (i.e., α- and β-$NaYF_4$ without any gold NPs) do not show any measurable catalytic activity (Figures 7 and 8).

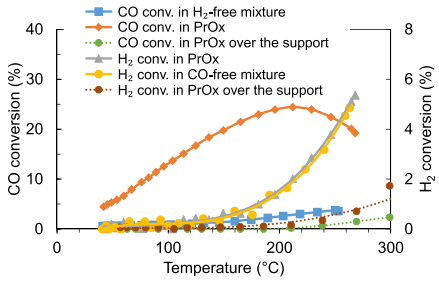

Figure 8. CO and H_2 conversion as a function of temperature over the β-$NaYF_4$ support and the Au/β-$NaYF_4$:Gd^{3+} catalyst in a H_2-free mixture (2% CO + 2% O_2 + 96% He), PrOx mixture (2% CO + 48% H_2 + 2% O_2 + 48% He), and CO-free mixture (48% H_2 + 2% O_2 + 50% He). All percentages are vol %.

For the sake of clarity and brevity, only the data corresponding to the second cooling steps are plotted and used for ensuing discussion. In Figure 8, the activity of Au/β-$NaYF_4$:Gd^{3+} as a function of temperatures is displayed. In the absence of H_2, oxidation of CO proceeds via a difficult O_2 dissociation step and, therefore, the oxidation rate observed is very low (4% CO conversion at 250 °C). The corresponding calculated rate per surface atom (TOF) is about 3 orders of magnitude lower than those observed for the usual metal oxide-supported gold NPs (e.g., Au/TiO_2 or Au/Fe_2O_3 reference catalysts). In the course of our previous investigation of PrOx (preferential oxidation) reaction on supported gold catalysts, we focused on the effect of H_2 addition on CO oxidation and demonstrated that the CO oxidation pathway was significantly altered in the presence of H_2.[32] Indeed, even a low H_2 amount added to a CO + O_2 feed accelerated the CO oxidation. In the present study also, the introduction of hydrogen in the reactant feed results in an increase of the CO

DOI: 10.1021/acsomega.9b00173
ACS Omega 2019, 4, 5852−5861

oxidation rate, as observed previously over the unsupported or alumina-supported gold catalysts.[33]

In the present case, the PrOx reaction proceeds with the highest selectivity toward CO at low temperature (nearly no water is formed up to 60 °C). This shows that the O_2 activation step, which is rate-determining in the CO−O_2 mixtures, is facilitated in PrOx mixtures, irrespective of whether the gold catalyst is unsupported or supported on oxide or "nonoxide" materials. As the temperature increases, hydrogen also commences to be oxidized to form water and, therefore, starts competing with CO for the reaction with oxygen. From our previous work on CO oxidation and PrOx,[32,33] it becomes clear that gold-catalyzed CO oxidation reactions advance in different ways depending on whether hydrogen is present in the feed or not. The presence of hydrogen accelerates CO oxidation, which suggests the involvement of different reactive species and, therefore, change in the kinetics and mechanism of the reaction. We have previously suggested the gold−hydroperoxy (Au−OOH) species as the critical oxidizing species and proposed a comprehensive mechanism where the molecularly adsorbed O_2 on Au is activated by H_2 to form OOH and H species.[34] This mechanism does not require O_2 dissociation on Au, which is known to be a highly activated step. Hence, introducing H_2 in a CO + O_2 mixture opens channels that cause O_2 to hydrogenate and dissociate thus easily to provide O for CO oxidation.

The behavior of the three other gold catalysts was very similar to the one that we described above and, therefore, will not be commented upon in detail. The TOF values of the four catalysts in the complete temperature range for CO conversion in PrOx conditions are reported in Figure 9. While comparing

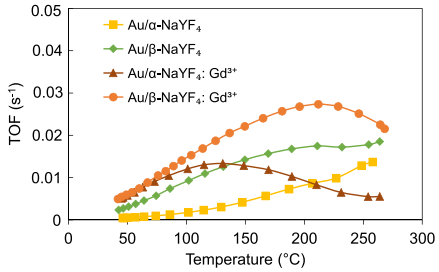

Figure 9. CO_2 production in TOF vs temperature over the four catalysts in the preferential oxidation of CO (PrOx: 2% CO + 2% O_2 + 48% H_2 + 48% He).

the activities of the different catalysts at low temperature (in the H_2 environment and temperature above 80 °C, water begins to form which competes with the conversion of CO), it becomes clear that the activity of the gold NPs is directly affected by the nature of the support. The following observations can be made: The doped catalysts Au/α-$NaYF_4$:Gd^{3+} and Au/β-$NaYF_4$:Gd^{3+} are nearly equal and superior to the Au/β-$NaYF_4$ catalyst which, in turn, is better than the Au/α-$NaYF_4$ catalyst. However, one has to note that even the highest value of TOF for these nonoxide-supported catalysts (~0.027 s^{-1} for Au/β-$NaYF_4$:Gd^{3+} at 210 °C) is once again low as compared to those shown by efficient metal oxide-supported gold NPs. These turnover values are of the same order of magnitude as those obtained on both unsupported or nanoporous gold powders in the presence of H_2.[33,34] The fact that these catalysts can be used for several reaction cycles without showing much difference in their reactivity underlines their stability and durability. As mentioned earlier, the activity of these catalysts enhanced after the first run, apparently because of the combustion of the inhibitory capping ligand PVA during the first heating cycle. In subsequent cycles, these catalysts showed almost similar reactivity. These catalysts did not show any appreciable change in the morphology of the support, though the mean diameters of the Au particles were found to be slightly larger in comparison to the fresh catalysts (Figures S12 and S13). Generally speaking, as compared to the methods employing reduction of grafted gold species to prepare the gold catalysts, the colloidal deposition method used here is expected to generate less strong interaction between the gold NPs and the support because this interaction is generated after the formation of Au NPs and, therefore, might lack strong covalent/ionic bonds. Nonetheless, the above observations on the morphology and the average gold particle size indicate that the Au−support interaction in the catalysts reported here is adequately strong to resist reasonably the floating and sintering of Au NPs when treated at an elevated temperature.

In conclusion, the metal fluoride-supported gold catalysts behaved on expected lines and exhibited a poor activity toward CO oxidation as compared to the gold catalysts supported on reducible metal oxides. The present study, however, confirmed the previous observation about a new way of CO oxidation being opened up in the presence of hydrogen. However, even with hydrogen, these gold catalysts on metal fluoride are found to be less efficient for activating oxygen than those supported on metal oxides.

3. CONCLUSIONS

Metal fluorides are evaluated as potential supports for gold catalysts. Using SSPs in a metal−organic decomposition process, NPs of two different crystalline phases of $NaYF_4$, namely α- and β-phases showing different surface characteristics, were prepared. The deposition of about 5 nm gold NPs on these heterometal fluorides, either undoped or doped with Gd^{3+} ions, generates efficient catalysts Au/α-$NaYF_4$, Au/β-$NaYF_4$, Au/α-$NaYF_4$:Gd^{3+}, and Au/β-$NaYF_4$:Gd^{3+} for the aerobic oxidation of *trans*-stilbene. These catalysts are either at par (in terms of the *trans*-stilbene oxide yield) or better (in terms of stilbene conversion) than the WGC reference catalyst Au/TiO_2. Doping the support $NaYF_4$ with Gd^{3+} eliminates the induction period and also enhances the catalytic activity, as indicated by larger TOF values, but decreases the selectivity. These results indicate that the composition and chemical nature of the support have little effect on the intrinsic epoxidation activity of the catalyst but rather influence the overall reactivity patterns via mass-transfer limitations. In contrast to the above epoxidation activity, these catalysts show poor activity for CO oxidation reactions, which can be accelerated to an extent by the presence of hydrogen. However, the overall activity of these metal fluoride-supported gold catalysts toward CO oxidation reactions remains less than those supported on metal oxides.

4. EXPERIMENTAL SECTION

4.1. General Procedures. All manipulations were carried out in an argon atmosphere using a Schlenk tube and vacuum line techniques. The purification of the solvents was achieved on an MB SPS-800 instrument. Fourier transform infrared

DOI: 10.1021/acsomega.9b00173
ACS Omega 2019, 4, 5852−5861

(FT-IR) spectra were recorded as KBr pellets on a Bruker Vector 22 spectrometer. SSPs [NaLn(TFA)$_4$(diglyme)] (Ln = Y, Gd) were prepared as described in our previous publications.[12] Powder XRD data were obtained with a Siemens D 5000 diffractometer using Cu Kα radiation. N_2 adsorption−desorption isotherms were obtained on an ASAP 2010 (Micromeritics) after desorbing the samples at 400 °C for 3 h. The TG−DTA data for the as-prepared $NaYF_4$ NPs were recorded in air on a Setaram 92 system in the temperature range 20−900 °C with a thermal ramp of 5 °C min^{-1}. TEM was performed on a JEOL JEM-2010 LaB6 microscope operated at 200 kV. The XPS analyses were carried out in a Kratos Ultra DLD spectrometer using a monochromatic Al Kα radiation [$Eh\nu$ (Al Kα) = 1486.6 eV (10 mA, 15 kV)] as the photon source. Survey scans were conducted in the binding energies between 1200 eV and 0 using a 1 eV step size, dwell time of 100 ms per step, and an analyser pass energy of 160 eV for all samples. All spectra were obtained at room temperature in the hybrid mode (combined electrostatic and magnetic lens) under ultrahigh vacuum (1×10^{-9} torr). The specific region photoelectron peaks, viz. O 1s, C 1s, F 1s, Na 1s, Y 3d, Gd 4d, Au 4f, and Si 2p, were scanned over an energy range of 20 eV with 0.1 eV step size. All photoelectron peaks were background-subtracted using a Shirley background and curve-fitted in the same manner, that is, a Lorentzian-to-Gaussian ratio of 30%. All spectra were then calibrated using the adventitious C 1s contaminant peak at 284.6 eV. Quantification was carried out with the VISION software supplied. The Au and Gd contents were determined by inductively coupled plasma−optical emission spectroscopy. The reference catalyst Au/TiO_2-WGC, purchased from WGC, was treated at 250 °C for 2 h in air before use. This treatment did not change its physicochemical properties (average Au diameter = 3.5 ± 0.9 nm, Au loading = 1.5 wt %).

4.2. Preparation of Cubic (α) and Hexagonal (β) Phases of $NaYF_4$ and $NaYF_4$:Gd^{3+} NPs. A typical method of obtaining α-$NaYF_4$ NPs involved taking the precursor [NaY(TFA)$_4$(diglyme)] in 1-octadecene (10 mL) and heating gradually at a rate of 10 °C/min in an inert atmosphere. After keeping at 250 °C for 1 h, the reaction mixture was allowed to cool to room temperature, and the NPs were then precipitated by adding ethanol and isolated via centrifugation. The obtained NPs were then washed two times by dispersing in ethanol, centrifugated, and dried at 70 °C (24 h). To obtain the α-$NaYF_4$ NPs doped with Gd^{3+}, the isostructural precursors [NaY(TFA)$_4$(diglyme)] and [NaGd(TFA)$_4$(diglyme)] were taken in about 20:1 ratio in 1-octadecene and then decomposed simultaneously.

When the above decomposition was carried out at the boiling temperature of 1-octadecene (i.e., 315 °C), it afforded $NaYF_4$ NPs with the mixed α- and β-phases, the latter phase being in the majority. These mixed-phase (α/β)-$NaYF_4$ and (α/β)-$NaYF_4$:Gd^{3+} NPs were calcined at 400 °C for 4 h in air to obtain the phase-pure β-$NaYF_4$ and β-$NaYF_4$:Gd^{3+} NPs, respectively.

4.3. Colloidal Gold Deposition. Au/α-$NaYF_4$, Au/β-$NaYF_4$, Au/α-$NaYF_4$:Gd^{3+}, and Au/β-$NaYF_4$:Gd^{3+} were prepared by colloidal deposition of gold over a suitable metal fluoride support, using 0.2 mL of a $HAuCl_4$ solution (0.25 mol L^{-1}) taken in 100 mL of deionized water, 1.3 mL of PVA solution (0.5 wt %, obtained by diluting PVA MW 10 000 in deionized water), 2.5 mL of a freshly prepared $NaBH_4$ solution (0.1 mol L^{-1}), and 1 g of metal fluoride support.[13] The as-obtained brownish to reddish catalysts were repeatedly washed with deionized water (1 L) as well as with ethanol and dried in air at 100 °C overnight. Gold loading was found in the range 0.72−0.94% by weight. The mean diameter for Au NPs, on the size distributions obtained from the TEM images, was in the range 5−6.5 nm. The gold dispersion was calculated via the determination of the volume/surface-weighted mean diameter d_{32}, also called the Sauter diameter. It was calculated from the particle size distribution histograms by the expression (eq 1)

$$d_{32} = \sum n_i d_i^3 / \sum n_i d_i^2 \quad (1)$$

One can relate the volume/surface-weighted mean diameter d_{32} to the dispersion D, which is the ratio of the number of surface atoms to the total number of atoms in the particle, by (eq 2)

$$D = (6 \cdot M)/(N_A \cdot \rho \cdot a \cdot d_{32}) \quad (2)$$

where M = atomic mass, N_A = Avogadro number, ρ = mass density of the particle, and a = surface area occupied by an atom on the particle surface.[35] a = 8.17 Å^2 for gold if one assumes equal proportions of the (111), (100), and (110) planes on the particle surface of this face-centered cubic metal.

4.4. Catalytic Evaluation. *4.4.1. Aerobic Epoxidation of trans-Stilbene.* Catalytic evaluation was studied in round-bottom flasks where *trans*-stilbene (1 mmol), the gold catalyst (Au: 2.1 ± 0.1 μmol), and an organic initiator (0.05 mmol/7 μL of a 70% TBHP in water Aldrich solution) were added to the solvent methylcyclohexane (20 mL/155 mmol) and stirred together (900 rpm) at 80 °C for over 60 h in air and at atmospheric pressure. The products resulting from the oxidation of stilbene were analyzed by high-performance liquid chromatography (PerkinElmer HPLC Series 200), using a Spheri-5 RP-18 220 mm × 4.6 mm × 3 μm C18 reverse-phase column, an acetonitrile/water mobile-phase mixture at a constant flow rate of 1.0 mL min^{-1} and a Series 200 UV detector set at 250 nm. External calibration was carried out by injecting standard solutions of *trans*-stilbene (96% Sigma-Aldrich) and *trans*-stilbene oxide (99% Sigma-Aldrich) in acetonitrile. Conversion, yield, selectivity, and TOFs are defined and calculated as explained in ref 13.

4.4.2. CO Oxidation. Using the same protocol, the catalysts were tested in three related reactions, the oxidation of CO (H_2-free), the selective oxidation of CO in the presence of H_2 (PrOx), and the oxidation of H_2 (CO-free). The tests were carried out in a continuous-flow fixed-bed reactor at atmospheric pressure. About 30 mg (between 10 and 45 mg) of the as-prepared material was loaded into a tube reactor in quartz (inner diameter = 3 mm), located in a ceramic furnace. No pretreatment was applied. The reactant flow consisted of a mixture of 2% CO + 2% O_2 + 96% He for the oxidation of CO, 2% CO + 2% O_2 + 48% H_2 + 48% He for the preferential oxidation of CO (PrOx), and 48% H_2 + 2% O_2 + 50% He for the oxidation of H_2 (all percentages are vol %). All the high-purity (>99.995%) gases were purchased from Air Liquide. Feed mixtures were generated at a typical flow rate of 50 N mL min^{-1} using mass-flow controllers (Brooks). The reactor was heated to 250 °C and then cooled to 25 °C at a heating (and cooling) rate of 1 °C min^{-1}. We carried out the product analysis online with a Varian-Micro GC (CP2003) equipped with a thermal conductivity detector.[32a]

DOI: 10.1021/acsomega.9b00173
ACS Omega 2019, 4, 5852−5861

■ ASSOCIATED CONTENT

Supporting Information

The Supporting Information is available free of charge on the ACS Publications website at DOI: 10.1021/acsomega.9b00173.

FT-IR spectrum and TG−DTA curves of the as-prepared $NaYF_4$ NPs; powder XRD, EDX, N_2 adsorption−desorption isotherms, and wide-scan XPS spectra of the newly synthesized Au/$NaYF_4$ catalysts; and XRD and TEM characterization of Au/α-$NaYF_4$ after catalysis (PDF)

■ AUTHOR INFORMATION

Corresponding Author

*E-mail: shashank.mishra@ircelyon.univ-lyon1.fr. Fax: +33-472445399.

ORCID

Shashank Mishra: 0000-0003-2846-4221

Notes

The authors declare no competing financial interest.

■ ACKNOWLEDGMENTS

We thank M. Aouine and L. Burel for TEM, Dr. L. Cardenas for XPS, F. Bosselet for XRD, as well as P. Mascunan for the elemental analyses. We also thank Dr V. Caps for the useful discussion on the part of epoxidation catalysis.

■ REFERENCES

(1) (a) Qian, L.; Wang, Z.; Beletskiy, E. V.; Liu, J.; dos Santos, H. J.; Li, T.; Rangel, M. D. C.; Kung, M. C.; Kung, H. H. Stable and solubilized active Au atom clusters for selective epoxidation of cis-cyclooctene with molecular oxygen. *Nat. Commun.* **2017**, *8*, 14881. (b) Vigneron, F.; Caps, V. Evolution in the chemical making of gold oxidation catalysts. *C. R. Chim.* **2016**, *19*, 192−198. (c) Liu, X.; He, L.; Liu, Y.-M.; Cao, Y. Supported gold catalysis: From small molecule activation to green chemical synthesis. *Acc. Chem. Res.* **2014**, *47*, 793−804. (d) Dimitratos, N.; Lopez-Sanchez, J. A.; Hutchings, G. J. Selective liquid phase oxidation with supported metal nanoparticles. *Chem. Sci.* **2012**, *3*, 20−44. (e) Corti, C. W.; Holliday, R. J.; Thompson, D. T. Progress towards the commercial application of gold catalysts. *Top. Catal.* **2007**, *44*, 331−343. (f) Hashmi, A. S. K.; Hutchings, G. J. Gold catalysis. *Angew. Chem., Int. Ed.* **2006**, *45*, 7896−7936.

(2) (a) Liu, X. Y.; Wang, A.; Zhang, T.; Mou, C.-Y. Catalysis by gold: New insights into the support effect. *Nano Today* **2013**, *8*, 403−416. (b) Liu, J. J. Advanced Electron Microscopy of Metal-Support Interactions in Supported Metal Catalysts. *ChemCatChem* **2011**, *3*, 934−948. (c) Rodriguez-González, V.; Zanella, R.; Calzada, L. A.; Gomez, R. Low-temperature CO oxidation and long-term stability of Au/In_2O_3−TiO_2 catalysts. *J. Phys. Chem. C* **2009**, *113*, 8911−8917. (d) Bokhimi, X.; Zanella, R. Crystallite size and morphology of the phases in Au/TiO_2 and Au/Ce-TiO_2 catalysts. *J. Phys. Chem. C* **2007**, *111*, 2525−2532.

(3) (a) Xiao, J.-D.; Han, L.; Luo, J.; Yu, S.-H.; Jiang, H.-L. Integration of Plasmonic Effects and Schottky Junctions into Metal-Organic Framework Composites: Steering Charge Flow for Enhanced Visible-Light Photocatalysis. *Angew. Chem., Int. Ed.* **2018**, *57*, 1103−1107. (b) Li, D.; Yu, S.-H.; Jiang, H.-L. From UV to Near-Infrared Light-Responsive Metal-Organic Framework Composites: Plasmon and Upconversion Enhanced Photocatalysis. *Adv. Mater.* **2018**, *30*, 1707377. (c) Yang, Q.; Jiang, H. L. Oxidation or Reduction State of Au Stabilized by an MOF: Active Site Identification for the Three-Component Coupling Reaction. *Small Methods* **2018**, *2*, 1800216. (d) Xu, H.; Li, Y.; Luo, X.; Xu, Z.; Ge, J. Monodispersed gold nanoparticles supported on a zirconium-based porous metal-organic framework and their high catalytic ability for the reverse water-gas shift reaction. *Chem. Commun.* **2017**, *53*, 7953−7956. (e) Jiang, H.-L.; Liu, B.; Akita, T.; Haruta, M.; Sakurai, H.; Xu, Q. Au@ZIF-8: CO Oxidation over Gold Nanoparticles Deposited to Metal−Organic Framework. *J. Am. Chem. Soc.* **2009**, *131*, 11302−11303. (f) Liu, H.; Liu, Y.; Li, Y.; Tang, Z.; Jiang, H. Metal−Organic Framework Supported Gold Nanoparticles as a Highly Active Heterogeneous Catalyst for Aerobic Oxidation of Alcohols. *J. Phys. Chem. C* **2010**, *114*, 13362−13369. (g) Zhang, X.; Ke, X.; Zhu, H. Zeolite-Supported Gold Nanoparticles for Selective Photooxidation of Aromatic Alcohols under Visible-Light Irradiation. *Chem.—Eur. J.* **2012**, *18*, 8048−8056. (h) Wang, S.; Wang, J.; Zhao, Q.; Li, D.; Wang, J.-Q.; Cho, M.; Cho, H.; Terasaki, O.; Chen, S.; Wan, Y. Highly Active Heterogeneous 3 nm Gold Nanoparticles on Mesoporous Carbon as Catalysts for Low-Temperature Selective Oxidation and Reduction in Water. *ACS Catal.* **2015**, *5*, 797−802.

(4) (a) Oh, S.; Kim, Y. K.; Jung, C. H.; Doh, W. H.; Park, J. Y. Effect of the metal-support interaction on the activity and selectivity of methanol oxidation over Au supported on mesoporous oxides. *Chem. Commun.* **2018**, *54*, 8174−8177. (b) Somorjai, G. A.; Frei, H.; Park, J. Y. Advancing the frontiers in nanocatalysis, biointerfaces, and renewable energy conversion by innovations of surface techniques. *J. Am. Chem. Soc.* **2009**, *131*, 16589−16605.

(5) (a) Machynskyy, O.; Kemnitz, E.; Karpiński, Z. Aluminum Fluoride-Supported Platinum and Palladium as Highly Efficient Catalysts ofn-Pentane Hydroisomerization. *ChemCatChem* **2014**, *6*, 592−602. (b) Negoi, A.; Wuttke, S.; Kemnitz, E.; Macovei, D.; Parvulescu, V. I.; Teodorescu, C. M.; Coman, S. M. One-Pot Synthesis of Menthol Catalyzed by a Highly Diastereoselective Au/MgF_2 Catalyst. *Angew. Chem., Int. Ed.* **2010**, *49*, 8134−8138.

(6) May, P. B.; Suter, J. D.; May, P. S.; Berry, M. T. The dynamics of nanoparticle growth and phase change during synthesis of β-$NaYF_4$. *J. Phys. Chem. C* **2016**, *120*, 9482−9489.

(7) (a) Grzechnik, A.; Bouvier, P.; Crichton, W. A.; Farina, L.; Köhler, J. Metastable $NaYF_4$ fluorite at high pressures and high temperatures. *Solid State Sci.* **2002**, *4*, 895−899. (b) Grzechnik, A.; Friese, K. Crystal structures and stability of $NaLnF_4$ (Ln = La, Ce, Pr, Nd, Sm and Gd) studied with synchrotron single-crystal and powder diffraction. *Dalton Trans.* **2012**, *41*, 10258−10266.

(8) (a) Mishra, S.; Mendez, V.; Jeanneau, E.; Caps, V.; Daniele, S. A Single Source Precursor Route to Group 13 Homo- and Heterometallic Oxides as Highly Active Supports for Gold-Catalyzed Aerobic Epoxidation oftrans-Stilbene. *Eur. J. Inorg. Chem.* **2013**, *2013*, 500−510. (b) Mishra, S.; Jeanneau, E.; Daniele, S.; Mendez, V. Aminoalkoxo-supported heteroleptic hexanuclear gallium(III) wheel as a synthon for group 13 heterometallics: A rare sol-gel precursor for mixed Al-Ga oxide as a support for gold catalysts. *Dalton Trans.* **2010**, *39*, 7440−7443.

(9) (a) Gahlot, S.; Jeanneau, E.; Dappozze, F.; Guillard, C.; Mishra, S. Precursor-mediated synthesis of $Cu_{2-x}Se$ nanoparticles and its composites with TiO_2 for improved photocatalysis. *Dalton Trans.* **2018**, *47*, 8897−8905. (b) Soussi, K.; Mishra, S.; Jeanneau, E.; Mantoux, A.; Daniele, S. Synthesis, characterization and thermal transport properties of heteroleptic N -alkyl triazenide complexes of titanium(IV) and niobium(V). *Polyhedron* **2018**, *152*, 84−89. (c) Soussi, K.; Mishra, S.; Jeanneau, E.; Millet, J.-M. M.; Daniele, S. Asymmetrically substituted triazenes as poor electron donor ligands in the precursor chemistry of iron(II) for iron-based metallic and intermetallic nanocrystals. *Dalton Trans.* **2017**, *46*, 13055−13064. (d) Mishra, S.; Du, D.; Jeanneau, E.; Dappozze, F.; Guillard, C.; Zhang, J.; Daniele, S. A Facile Molecular Precursor-based Synthesis of Ag_2Se Nanoparticles and Its Composites with TiO_2 for Enhanced Photocatalytic Activity. *Chem.−Asian J.* **2016**, *11*, 1658−1663. (e) Mishra, S.; Jeanneau, E.; Rolland, M.; Daniele, S. Structural isomers of iron(III) *N*-methyl diethanolaminate as sol-gel precursors for iron-based oxide nanomaterials. *RSC Adv.* **2016**, *6*, 1738−1743. (f) Mishra, S.; Jeanneau, E.; Mangematin, S.; Chermette, H.; Poor Kalhor, M.; Bonnefont, G.; Fantozzi, G.; Le Floch, S.; Pailhes, S.; Daniele, S. A convenient and quantitative route to Sn(iv)-M [M =

DOI: 10.1021/acsomega.9b00173
ACS Omega 2019, 4, 5852−5861

Ti(iv), Nb(v), Ta(v)] heterobimetallic precursors for dense mixed-metal oxide ceramics. *Dalton Trans.* **2015**, *44*, 6848−6862. (g) Mishra, S.; Jeanneau, E.; Berger, M.-H.; Hochepied, J.-F.; Daniele, S. Novel heteroleptic heterobimetallic alkoxide complexes as facile single-source precursors for Ta^{5+}-doped TiO_2-SnO_2 nanoparticles. *Inorg. Chem.* **2010**, *49*, 11184−11189. (h) Mishra, S.; Daniele, S.; Hubert-Pfalzgraf, L. G. Metal 2-ethylhexanoates and related compounds as useful precursors in materials science. *Chem. Soc. Rev.* **2007**, *36*, 1770−1787.

(10) Mishra, S.; Daniele, S. Metal-organic derivatives with fluorinated ligands as precursors for inorganic nanomaterials. *Chem. Rev.* **2015**, *115*, 8379−8448.

(11) (a) Mishra, S.; Jeanneau, E.; Bulin, A.-L.; Ledoux, G.; Jouguet, B.; Amans, D.; Belsky, A.; Daniele, S.; Dujardin, C. A molecular precursor approach to monodisperse scintillating CeF_3 nanocrystals. *Dalton Trans.* **2013**, *42*, 12633−12643. (b) Ayadi, H.; Fang, W.; Mishra, S.; Jeanneau, E.; Ledoux, G.; Zhang, J.; Daniele, S. Influence of Na^+ ion doping on the phase change and upconversion emissions of the GdF_3: Yb^{3+}, Tm^{3+} nanocrystals obtained from the designed molecular precursors. *RSC Adv.* **2015**, *5*, 100535−100545.

(12) (a) Chen, Y.; Mishra, S.; Ledoux, G.; Jeanneau, E.; Daniel, M.; Zhang, J.; Daniele, S. Direct synthesis of hexagonal $NaGdF_4$ nanocrystals from a single-source precursor: Upconverting NaGd-F_4:Yb^{3+},Tm^{3+} and its composites with TiO_2 for near-IR-driven. *Chem.—Asian J.* **2014**, *9*, 2415−2421. (b) Mishra, S.; Ledoux, G.; Jeanneau, E.; Daniele, S.; Joubert, M.-F. Novel heterometal-organic complexes as first single source precursors for up-converting $NaYF_4$:Yb^{3+}, Er^{3+}/Tm^{3+} nanomaterials. *Dalton Trans.* **2012**, *41*, 1490−1502. (c) Mishra, S.; Daniele, S.; Ledoux, G.; Jeanneau, E.; Joubert, M.-F. Heterometallic Na-Y(Ln) trifluoroacetate diglyme complexes as novel single source precursors for upconverting $NaYF_4$ nanocrystals co-doped with Yb and Er/Tm ions. *Chem. Commun.* **2010**, *46*, 3756−3758.

(13) Mendez, V.; Guillois, K.; Daniele, S.; Tuel, A.; Caps, V. Aerobic methylcyclohexane-promoted epoxidation of stilbene over gold nanoparticles supported on Gd-doped titania. *Dalton Trans.* **2010**, *39*, 8457−8463.

(14) (a) Shannon, R. D. Revised effective ionic radii and systematic studies of interatomic distances in halides and chalcogenides. *Acta Crystallogr., Sect. A: Cryst. Phys., Diffr., Theor. Gen. Crystallogr.* **1976**, *32*, 751−767. (b) Wang, F.; Han, Y.; Lim, C. S.; Lu, Y.; Wang, J.; Xu, J.; Chen, H.; Zhang, C.; Hong, M.; Liu, X. Simultaneous phase and size control of upconversion nanocrystals through lanthanide doping. *Nature* **2010**, *463*, 1061−1065.

(15) Zhao, J.; Liu, X.; Cui, D.; Sun, Y.; Yu, Y.; Yang, Y.; Du, C.; Wang, Y.; Song, K.; Liu, K.; Lu, S.; Kong, X.; Zhang, H. A facile approach to fabrication of hexagonal-phase $NaYF_4$:Yb^{3+}, Er^{3+} hollow nanospheres: Formation mechanism and upconversion luminescence. *Eur. J. Inorg. Chem.* **2010**, *2010*, 1813−1819.

(16) Genet, M.; Dupont-Gillain, C. C.; Rouxhet, P. XPS analysis of biosystems and biomaterials In *Medical Applications of Colloids*; Matijevic, E., Ed.; Springer: New York, 2008; Chapter 5, pp 177−307.

(17) Visco, A. M.; Neri, F.; Neri, G.; Donato, A.; Milone, C.; Galvagno, S. X-ray photoelectron spectroscopy of Au/Fe_2O_3 catalysts. *Phys. Chem. Chem. Phys.* **1999**, *1*, 2869−2873.

(18) Duo, S.; Zhong, C.; Zhang, J.; Liu, Z.; Zhong, R.; Liu, T. Preparation of $NaYF_4$: Gd^{3+}, Yb^{3+}, Tm^{3+} @ TiO_2 and $NaYF_4$: Gd^{3+}, Yb^{3+}, Tm^{3+} @ TiO_2 @ Au nanocomposites and their upconversion and photocatalytic properties under simulated solar light with or without an UV filter. *J. Mater. Sci.: Mater. Electron.* **2018**, *29*, 2974−2987.

(19) Tripathy, P.; Mishra, A.; Ram, S.; Fecht, H.-J.; Bansmann, J.; Behm, R. J. X-ray photoelectron spectrum in surface interfacing of gold nanoparticles with polymer molecules in a hybrid nanocomposite structure. *Nanotechnology* **2009**, *20*, 075701.

(20) Lignier, P.; Comotti, M.; Schüth, F.; Rousset, J.-L.; Caps, V. Effect of the titania morphology on the Au/TiO_2-catalyzed aerobic epoxidation of stilbene. *Catal. Today* **2009**, *141*, 355−360.

(21) Arrii, S.; Morfin, F.; Renouprez, A. J.; Rousset, J. L. Oxidation of CO on gold supported catalysts prepared by laser vaporization: Direct evidence of support contribution. *J. Am. Chem. Soc.* **2004**, *126*, 1199−1205.

(22) Lignier, P.; Mangematin, S.; Morfin, F.; Rousset, J.-L.; Caps, V. Solvent and oxidant effects on the Au/TiO_2-catalyzed aerobic epoxidation of stilbene. *Catal. Today* **2008**, *138*, 50−54.

(23) Guillois, K.; Mangematin, S.; Tuel, A.; Caps, V. Gold-catalyzed aerobic epoxidation of *trans*-stilbene in methylcyclohexane. Part II: Identification and quantification of a key reaction intermediate. *Catal. Today* **2012**, *203*, 111−115.

(24) Bawaked, S.; Dummer, N. F.; Bethell, D.; Knight, D. W.; Hutchings, G. J. Solvent-free selective epoxidation of cyclooctene using supported gold catalysts: an investigation of catalyst re-use. *Green Chem.* **2011**, *13*, 127−134.

(25) Hardeveld, R. V.; Hartog, F. The statistics of surface atoms and surface sites on metal crystals. *Surf. Sci.* **1969**, *15*, 189−230.

(26) Kerdi, F.; Caps, V.; Tuel, A. Mesostructured Au/C materials obtained by replication of functionalized SBA-15 silica containing highly dispersed gold nanoparticles. *Microporous Mesoporous Mater.* **2011**, *140*, 89−96.

(27) Gajan, D.; Guillois, K.; Delichère, P.; Basset, J.-M.; Candy, J.-P.; Caps, V.; Coperet, C.; Lesage, A.; Emsley, L. Gold nanoparticles supported on passivated silica: Access to an efficient aerobic epoxidation catalyst and the intrinsic oxidation activity of gold. *J. Am. Chem. Soc.* **2009**, *131*, 14667−14669.

(28) Haruta, M.; Kobayashi, T.; Sano, H.; Yamada, N. Novel Gold Catalysts for the Oxidation of Carbon Monoxide at a Temperature far Below 0 °C. *Chem. Lett.* **1987**, *16*, 405−408.

(29) Prati, L.; Martra, G. New gold catalysts for liquid phase oxidation. *Gold Bull.* **1999**, *32*, 96−101.

(30) Singh, J. A.; Overbury, S. H.; Dudney, N. J.; Li, M.; Veith, G. M.; Gabriel, M.; Veith, G. M. Gold nanoparticles supported on carbon nitride: Influence of surface hydroxyls on low temperature carbon monoxide oxidation. *ACS Catal.* **2012**, *2*, 1138−1146.

(31) (a) Comotti, M.; Li, W.-C.; Spliethoff, B.; Schüth, F. Support effect in high activity gold catalysts for CO oxidation. *J. Am. Chem. Soc.* **2006**, *128*, 917−924. (b) Li, Y.; Zheng, Y.; Wang, L.; Fu, Z. Oxidative esterification of methacrolein to methyl methacrylate over supported gold catalysts prepared by colloid deposition. *ChemCatChem* **2017**, *9*, 1960−1968.

(32) (a) Rossignol, C.; Arrii, S.; Morfin, F.; Piccolo, L.; Caps, V.; Rousset, J.-L. Selective oxidation of CO over model gold-based catalysts in the presence of H_2. *J. Catal.* **2005**, *230*, 476−483. (b) Quinet, E.; Morfin, F.; Diehl, F.; Avenier, P.; Caps, V.; Rousset, J.-L. Hydrogen effect on the preferential oxidation of carbon monoxide over alumina-supported gold nanoparticles. *Appl. Catal., B* **2008**, *80*, 195−201.

(33) (a) Quinet, E.; Piccolo, L.; Daly, H.; Meunier, F. C.; Morfin, F.; Valcarcel, A.; Diehl, F.; Avenier, P.; Caps, V.; Rousset, J.-L. H_2-induced promotion of CO oxidation over unsupported gold. *Catal. Today* **2008**, *138*, 43−49. (b) Déronzier, T.; Morfin, F.; Massin, L.; Lomello, M.; Rousset, J.-L. Pure nanoporous gold powder: Synthesis and catalytic properties. *Chem. Mater.* **2011**, *23*, 5287−5289.

(34) Quinet, E.; Piccolo, L.; Morfin, F.; Avenier, P.; Diehl, F.; Caps, V.; Rousset, J.-L. On the mechanism of hydrogen-promoted gold-catalyzed CO oxidation. *J. Catal.* **2009**, *268*, 384−389.

(35) Bergeret, G. In *Catalysis by Metals*; Renouprez, A. J., Jobic, H., Eds.; Springer: Berlin, 1997; p 167.

DOI: 10.1021/acsomega.9b00173
ACS Omega 2019, 4, 5852−5861